Thermal behavior of apatitic calcium phosphates synthesized from calcium carbonate and orthophosphoric acid or potassium dihydrogen orthophosphate

Doan Pham Minh, Marta Galera Martinez, Ange Nzihou, Patrick Sharrock

Thermal behavior of apatitic calcium phosphates synthesized from calcium carbonate and orthophosphoric acid or potassium dihydrogen orthophosphate

Doan Pham Minh · Marta Galera Martínez · Ange Nzihou · Patrick Sharrock

Abstract The synthesis of calcium hydroxyapatite powder (Ca-HA) from orthophosphoric acid or from potassium dihydrogen orthophosphate and calcium carbonate was carried out under moderate conditions. A better dissolution of calcium carbonate and a complete precipitation of the orthophosphate species were obtained with orthophosphoric acid, indicating that it may be of interest as a phosphate source compared with potassium dihydrogen orthophosphate. The influence of calcination treatment on the physico-chemical properties of the solids is discussed in this paper. Different characterization techniques such as specific surface area (S_{BET}), true density, particle size distribution, thermo-mechanical analysis, simultaneous thermogravimetry and differential scanning calorimetry analysis, X-ray diffraction and infrared were performed to understand the phase changes during thermal treatment. Specific surface area decreased while true density and particle size increased with the rise in the calcination temperature, due to the sintering of particles and the chemical reactions occurring at high temperatures. Mixtures of well-crystallized Ca-HA and tricalcium phosphate (TCP) or well-crystallized Ca-HA, CaO, and TCP were obtained after calcination at 800–1,000 °C of the solid products starting from orthophosphoric acid or potassium dihydrogen orthophosphate, respectively.

D. Pham Minh (✉) · M. Galera Martínez · A. Nzihou
Université de Toulouse, Mines Albi, CNRS, Centre RAPSODEE, Campus Jarlard, 81013 Albi Cedex 09, France
e-mail: doan.phamminh@mines-albi.fr

P. Sharrock
Université de Toulouse, SIMAD, IUT Paul Sabatier, Avenue Georges Pompidou, 81104 Castres, France

Keywords Apatite · Calcium hydroxyapatite · Calcium carbonate · Thermal treatment

Introduction

Calcium orthophosphates form a large family of chemical compounds including dicalcium phosphate dihydrate (DCPD, $CaHPO_4{\cdot}2H_2O$); dicalcium phosphate anhydrous (DCPA, $CaHPO_4$); octacalcium phosphate ($Ca_8(HPO_4)_2(PO_4)_4{\cdot}5H_2O$); β-tricalcium phosphate (β-TCP, $Ca_3(PO_4)_2$); or calcium hydroxyapatite (Ca-HA, $Ca_{10}(PO_4)_6(OH)_2$). In this family, Ca-HA seems to be the most widely studied, because of its excellent properties, such as biocompatibility, bioactivity, and osteoconductivity [1], and its high-potential application in different fields such as catalysis, heavy metal removal, gas sensors, or chromatography [2].

Generally, low-crystallinity Ca-HA is prepared by the precipitation of calcium cations with orthophosphate anions under mild conditions [3, 4]. In the biomaterials field, low-crystallinity Ca-HA is usually converted into pure and well-crystallized Ca-HA by a calcination step at high temperature [5, 6]. Ca-HA used in gas sensors is also treated by a thermal process [7]. In heterogeneous catalysis, the activation of Ca-HA usually takes place at high temperature. For example, methane dry reforming was successfully carried out at 600 °C into a mixture of CO and H_2 over nickel-loaded Ca-HA, which was pre-treated at 800 °C [8]. Propane oxidative dehydrogenation into propene was carried out over an iron–Ca-HA catalyst system, in which the conversion of propane and the selectivity of the catalyst strongly depended on the reaction temperature in the range of 350–550 °C [9]. Thermal treatment probably leads to a change in the physico-chemical properties of Ca-HA, such as specific surface area, porosity, density,

particle size, crystallinity, etc. However, this is not always discussed.

In the present study, we report the thermal behavior of apatitic calcium phosphates obtained from calcium carbonate and orthophosphoric acid or potassium dihydrogen orthophosphate. Calcium carbonate is considered as the most available calcium source. H_3PO_4 and KH_2PO_4 were chosen as the most common orthophosphate sources. Understanding the thermal behavior of the synthesized apatitic products allows to anticipate their effective use in high temperature processes such as in heterogeneous catalysis or treatment of polluted gas. Products made with these starting materials showed equivalent reactivity in the removal of lead(II) from an aqueous solution to that obtained with classical Ca-HA produced from water soluble precursors of calcium [10].

Experimental

Apatitic calcium phosphates were synthesized by the precipitation of orthophosphate anions in an aqueous solution by adding calcium carbonate powder under ambient conditions (ca. 25 °C and 1 bar). Calcium carbonate in fine powder form from Fisher Scientific ($CaCO_3$, 98 %) was used as a calcium source. Orthophosphoric acid (H_3PO_4, 85 wt% in water, Merck) and potassium dihydrogen orthophosphate (KH_2PO_4, 99 %, Fisher Scientific) were used as orthophosphate sources.

For the preparation, 0.6 mol of H_3PO_4 (SYN-H) or KH_2PO_4 (SYN-K) and 400 ml of water were fed into 1.2 l U-form glass reactor (id: 10 cm; length: 15 cm), which was equipped with a vertical stainless steel stirrer. Then, 1.0 mol of $CaCO_3$ were progressively added to the orthophosphate solution. The homogeneity of the reaction mixture was assured by a two-blade stirrer inside the reactor vessel which ran at 400 rpm. The reaction mixture was kept for 48 h under stirring. The pH of the reaction mixture was measured using a Mettler–Toledo S20 SevenEasy pH-meter. Samples withdrawn at different times from the reactor were filtered on a 0.45 μm filter paper to separate liquid and solid phases. The solid was dried overnight at 105 °C under air atmosphere and the liquid was acidified with concentrated nitric acid to avoid further precipitation of soluble calcium and orthophosphate ions.

The calcination of the solid was performed in a Nabertherm P320 muffle with a heating rate of 10 °C min^{-1}. When the muffle reached the desired temperature in the range of 400–1,000 °C, the solid was kept at this temperature for 5 h, and then allowed to cool down to room temperature. In parallel, the thermal shrinkage of particle was also followed by thermo-mechanical analysis (TMA, Setaram Setsys 16/18) with 5 g of constant load on the powder sample under air atmosphere.

In order to investigate the changes due to the thermal treatment, different characterizations and analysis methods were used. Crystal phases were identified using the X-ray diffraction (XRD) technique on a Phillips Panalytical X'pert Pro MPD diffractometer with a Cu K_α (1.543 Å) radiation source and a nickel filter to suppress the Cu K_β ray. The texture and morphology of the particles were analyzed by scanning electron microscopy (SEM) on a Philips XL30 ESEM apparatus (FEI). Particle-size distribution was measured by laser scattering in a Mastersizer 2000 (Malvern Instruments Ltd., Malvern, UK) in the range of 0.020–2,000 μm. Specific surfaces areas were measured using the BET method by nitrogen adsorption on a Micrometrics Gemini Vacprep 061. The adsorption–desorption isotherms were measured with a Micrometrics ASAP 2010 using nitrogen as gas adsorbate with the data collection from relative pressure ($P/P°$) of 0.03–0.99. Simultaneous thermogravimetry and differential scanning calorimetry analysis (TG–DSC) were performed in a TA Instruments SDTQ600 analyzer with a heating rate of 5 °C min^{-1} under air flux (100 mL min^{-1}). Infrared spectroscopy (IR) was recorded on a Shimadzu FTIR 8400S spectrometer using a sensitive pyroelectric detector with an L-alanine-doped deuterated triglycine sulfate element. True density of the solid powders was measured by helium pycnometry using an Accupyc 1330 (Micromeritics).

After acidification with concentrated nitric acid, the liquid fraction was analyzed by inductively coupled plasma atomic emission spectroscopy (ICP-AES) using a HORIBA Jobin–Yvon Ultima 2 for determination of soluble elemental concentration of potassium, phosphorus, and calcium.

Results and discussion

In this section, the solids obtained after 48 h of reaction from the syntheses using orthophosphoric acid and potassium dihydrogen orthophosphate are labeled as SYN-H solids and SYN-K solids, respectively. They were either dried at 105 °C or calcined at 400–1,000 °C before all further characterizations.

Elemental analysis of the liquid phase

Much work has been done on the synthesis of Ca-HA but most reports did not study the composition of the liquid phase. In other words, the yield of the synthesis process was not calculated, although it was an important parameter to evaluate the performance of the synthesis process.

Table 1 shows the quantity of soluble calcium and phosphorus in the liquid phase analyzed by the ICP-AES

technique. In both syntheses, the quantity of initial soluble phosphorus present in the reactor at time zero was 600 mmol. In SYN-H using orthophosphoric acid, soluble orthophosphate species were completely precipitated after 1 h of contact with calcium carbonate at ambient conditions. When potassium dihydrogen orthophosphate was used (SYN-K), the precipitation of orthophosphate species was not complete. 241 mmol (or 40 %) of the initial soluble phosphorus remained in liquid phase after 48 h of contact. On the other hand, the content of soluble calcium in liquid phase was nearly negligible in both syntheses. This means that most calcium existed in solid phases which could be either precipitates of calcium phosphates or non-dissolved calcium carbonate. Similar results were obtained for the elemental analysis of the solid phase.

TG–DSC analysis

Figure 1 presents the derivative thermogravimetry (DTG) and DSC curves of the solid products obtained after 48 h of reaction and dried at 105 °C.

The dried SYN-H solid had different mass losses which corresponded to the following temperature at maximum DTG signals (DTG_{max}): 55, 112, 233, 419, 679, and 780 °C. The first mass loss at 55 °C was generally due to the removal of surface moisture. The next mass losses at 112, 233, and 419 °C could be attributed to the thermal decomposition of intermediates such as mono-calcium phosphate monohydrate (MCPM, $Ca(H_2PO_4)_2{\cdot}H_2O$), DCPD, and DCPA, which are usually formed in the synthesis of Ca-HA from the precipitation of orthophosphate anions in similar synthesis conditions [11, 12]. The mass loss at 679 °C corresponded to the decarbonation of the calcium carbonate remaining in the dried solid product. The final mass loss at 780 °C could be attributed to the decarbonation of calcium carbonate-containing apatite (CAP) [13, 14]. It has been shown that CAP can be formed when the crystallization of Ca-HA takes place in the presence of carbonate anions [15, 16].

For the dried SYN-K solid, the removal of surface moisture happened continuously up to ca. 90 °C, indicating the possible presence of different types of physical adsorption of the moisture on the surface of the solid. No mass loss was recorded in the temperature range from 100 to 610 °C, except for a weak signal at about 233 °C. This suggests the absence—or the presence at very low content—of intermediates such as MCPM, DCPD, and DCPA in this solid. Two mass losses at 680 and 780 °C corresponded to the decarbonation of calcium carbonate and CAP, as observed above for SYN-H solid.

For both solids, all thermal transitions were endothermic. As regards the intensity of heat-flow signals, the dehydration step was the most significant. On the other hand, the decarbonation of calcium carbonate was thermally much less significant, although it constituted the greatest mass loss in the range of temperatures investigated.

From the TG curves in the temperature range of 600–700 °C, which corresponded to the thermal decomposition of calcium carbonate, the content of residual calcium carbonate could be calculated (Table 2). Orthophosphoric

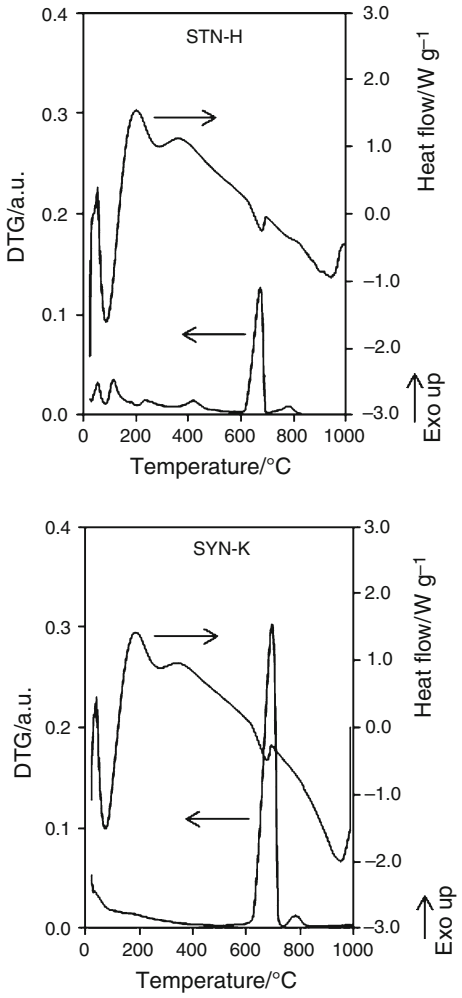

Fig. 1 DTG and DSC *curves* in the thermal analysis of the solids obtained after 48 h of reaction and dried at 105 °C

Table 1 ICP-AES analysis of calcium and phosphorus in liquid phase

Time/h	SYN-H		SYN-K	
	P/mmol	Ca/mmol	P/mmol	Ca/mmol
0	600	1000[a]	600	1000[a]
1	0.4	1.3	283	0.6
24	0.3	0.8	257	0.4
48	0.3	0.4	241	0.2

[a] Under initial solid powder form of $CaCO_3$

Table 2 Content of calcium carbonate remaining in the solids dried at 105 °C

Solid	DTG_{max}/°C	Residual $CaCO_3$/wt%
SYN-H, dried at 105 °C	679	11
SYN-K, dried at 105 °C	680	35

DTG_{max}, temperature at maximum of DTG signals

acid, with a higher acidity, led to a higher dissolution of calcium carbonate than did potassium dihydrogen orthophosphate under similar synthesis conditions.

XRD characterization

The identification of the crystalline phases using XRD characterization was carried out with the JCPDS database. The calcium carbonate used in this study was pure calcite without the presence of other calcium carbonate phases such as aragonite or vaterite. Figure 2 shows the XRD patterns of the solid products dried at 105 °C or calcined at different temperatures. For both solids obtained after 48 h of reaction and dried at 105 °C, most of the peaks could be attributed to low-crystallinity Ca-HA and crystalline calcite remained after the synthesis. The calcination at 400 °C for 5 h had no influence on the crystalline phase of these solids. When the calcination temperature was increased to 600 °C, all residual calcium carbonate decomposed into calcium oxide, and calcium pyrophosphate ($Ca_2P_2O_7$) appeared as a new crystalline phase. The formation of calcium pyrophosphate by the condensation of DCPD or DCPA has previously been observed [12, 17]. Calcium oxide was at higher intensity in the solid produced from SYN-K than in the solid coming from SYN-H, which was in accord with TG analysis. At this calcination temperature, Ca-HA seemed still to be of low crystallinity.

At higher temperatures, the behavior of the two solid products notably changed. For SYN-H solid calcined at 800 °C, well-crystallized tricalcium phosphate (TCP, Ca/P molar ratio of 1.5) appeared, and Ca-HA became more crystalline. At 1,000 °C, the TCP was virtually unchanged in comparison with the solid calcined at 800 °C, but well-crystallized Ca-HA was formed. Some trace of calcium oxide remained at both 800 and 1,000 °C. These results were in coherence with the elemental analysis. In fact, the solid from the reaction of orthophosphoric acid with calcium carbonate had the Ca/P molar ratio of 1.67. The calcination process used in this study did not allow a perfect homogeneity in the whole solid to totally convert calcium oxide and TCP into a Ca-HA structure.

For SYN-K using KH_2PO_4 as orthophosphate source, 40 % of initial orthophosphate species remained in the liquid phase (Table 1). Therefore, a higher Ca/P molar ratio in the resulting solid product was obtained, which was of 2.78. Thus, well-crystallized Ca-HA was formed at 800 and 1,000 °C as the only crystalline calcium phosphate. Calcium oxide remained at high content in this solid because of its high Ca/P molar ratio.

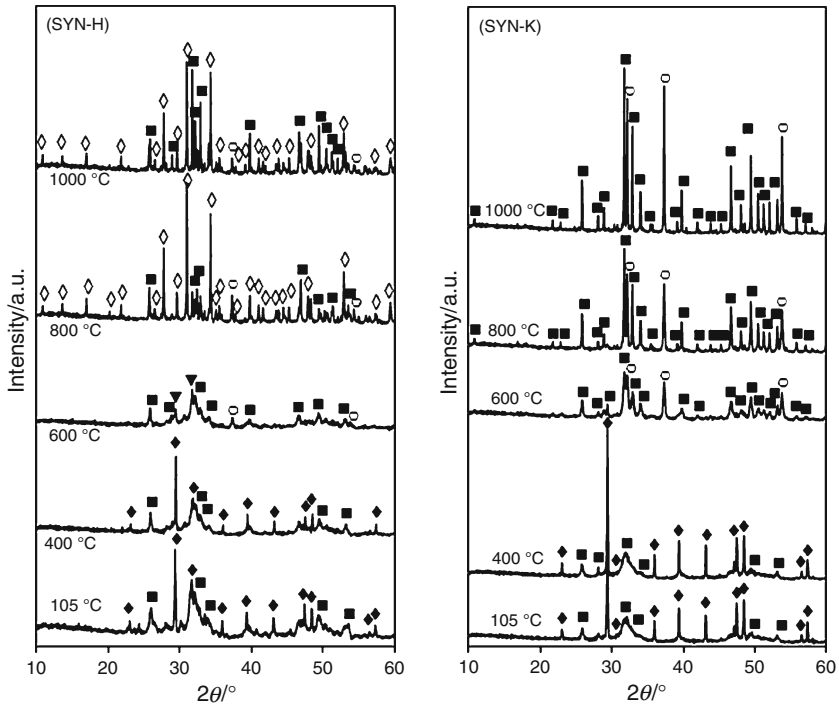

Fig. 2 XRD patterns of the solid powders treated at different temperatures; diffraction of: TCP $Ca_3(PO_4)_2$ (*open diamonds*); Ca-HA (*filled squares*); calcium carbonate (*filled diamonds*); calcium oxide CaO (*open circles*); calcium pyrophosphate $Ca_2P_2O_7$ (*filled down-pointing triangles*)

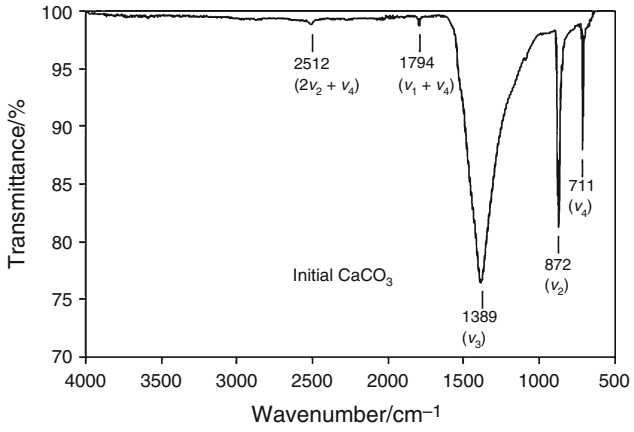

Fig. 3 IR spectrum of the initial calcium carbonate used in this study

IR analysis

Figure 3 presents the IR spectrum of the initial calcium carbonate used in this study. As expected, five net peaks appeared, at 711, 872, 1389, 1794, and 2512 cm^{-1}, which are the characteristic peaks of calcite [18–20].

Figure 4 illustrates the spectra of the solid products dried or calcined at different temperatures, and Table 3 summarizes the absorption bands present in Fig. 4 with the corresponding assignments [12, 15, 21–23].

In both SYN-H and SYN-K solids, the absorptions at 3,570 and 632 cm^{-1} of hydroxyl groups in well-crystallized Ca-HA appeared only at high calcination temperatures in the range of 600–1,000 °C, which were in coherence with XRD results.

The residual calcite completely decomposed in the calcination temperature range of 600–1,000 °C. As expected, the absorption at 711 cm^{-1}, which is one of the principal peaks of calcite (Fig. 3), appeared only in the solid dried at 105 °C or calcined at 400 °C. Exceptionally, low signals of calcite could also be observed in SYN-K solids after calcination at 800 and 1,000 °C, which can be explained by the presence of high amounts of CaO in these solids (Fig. 2). In contact with free air, trace amounts of calcite were probably formed.

The carbonate group in the CAP structure was characterized by the bi-modal peak at 1,454/1,405 cm^{-1} [15], which was not observed in SYN-H solids. On the other hand, a signal clearly appeared in SYN-K solid dried at 105 °C, and its intensity progressively decreased with the increase of the calcination temperature. In fact, after 48 h of reaction, the final pH of the reaction mixture was of 8.4 and 6.8 for SYN-K and SYN-H syntheses, respectively. The concentration of (bi)carbonate anions must be higher in SYN-K than that in SYN-H. Thus, the formation of CAP was more favorable in SYN-K.

The absorption bands of the $P_2O_7^{4-}$ group at 1,218 and 727 cm^{-1} [21] were found only for SYN-H solid calcined at 600 °C. The absorption bands of the PO_4^{3-} group were found mostly in the ranges 1,100–930 and 570–601 cm^{-1}.

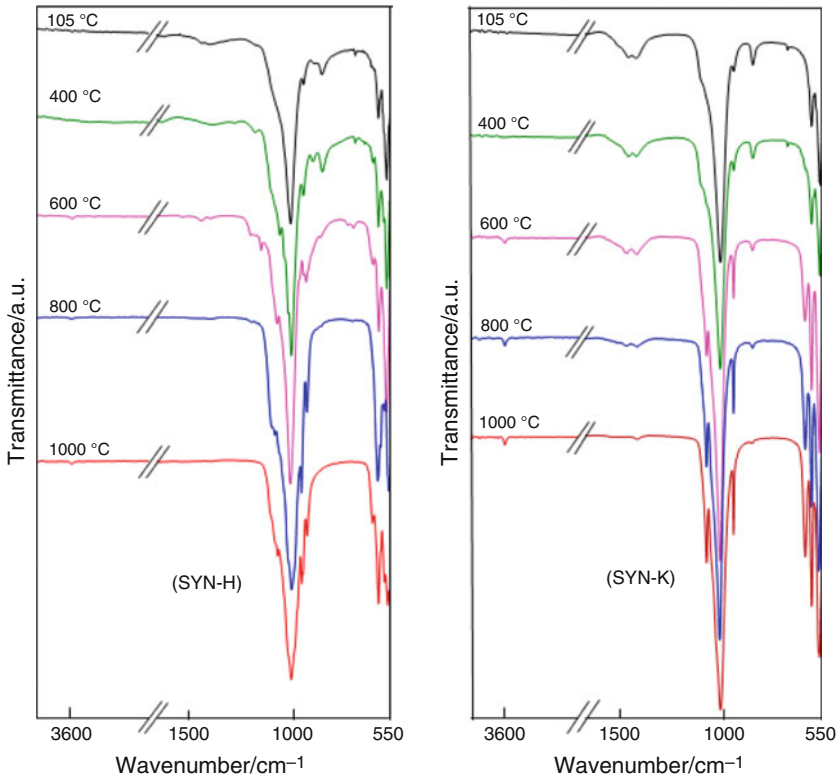

Fig. 4 IR spectra of the solid products treated at different temperatures

Table 3 IR peaks and assigned compounds for the spectra shown in Fig. 4

Wavenumber/cm^{-1}	Assignment
3570	OH stretch
632	OH libration
1389, 872, 711	CO_3^{2-} (calcite)
1454, 1405	CO_3^{2-} (CAP), v_3 mode
1218	$P_2O_7^{4-}$ (pyrophosphate), P=O stretch
727	$P_2O_7^{4-}$ (pyrophosphate), P–O–P stretch
1087, 1032	PO_4^{3-}, v_3 mode
962	PO_4^{3-}, v_1 mode
939	PO_4^{3-}, v_1 mode, TCP
601, 571	PO_4^{3-}, v_4 mode

The PO_4^{3-} group present in the Ca-HA structure was characterized by the absorptions at 1087, 1032, 962, 601, and 571 cm^{-1} [12], which were found for both SYN-H and SYN-K solids. For SYN-K solids calcined at 600–1,000 °C, no other peak of phosphate-based compounds was observed. This again confirmed the results of XRD characterization (Fig. 2) that Ca-HA was the only calcium phosphate present in these solids. For SYN-H solids, in addition to the absorption bands mentioned above for the PO_4^{3-} group in the Ca-HA structure, there was a peak at 938 cm^{-1} when the calcination temperature was between 800 and 1,000 °C, which was attributed to TCP [22].

Specific surface area and true density

The initial calcium carbonate used in this study had a negligible specific surface area (S_{BET}, smaller than 2 m^2 g^{-1}), and a true density of 2.68 g cm^{-3}. Figure 5 presents the evolution of S_{BET} (continuous lines) and true density (dotted lines) as functions of the calcination temperature. Despite the lower dissolution of calcium carbonate, the solid product coming from SYN-K using potassium dihydrogen orthophosphate had an initial S_{BET} of 103 m^2 g^{-1}, which was twice as much as that of the solid resulting from SYN-H using orthophosphoric acid (42 m^2 g^{-1}). Both solids continuously lost their S_{BET} as the calcination temperature increased. At 1,000 °C, their S_{BET} were very small, as found in dense non-porous solids.

Both solid products dried at 105 °C had a similar true density of 2.84 g cm^{-3}, which was higher than that of the initial $CaCO_3$. In parallel with the reduction of S_{BET}, the true density of both solids continuously increased. At 400 °C, the true density of both SYN-H and SYN-K solids was of 2.93 g cm^{-3}. In the range 600–1,000 °C, SYN-K solids were more compact than SYN-H solids calcined at the same temperature.

The changes in S_{BET} and true density during the calcination step were generally due to the sintering phenomenon, which has already been observed for the apatitic solid synthesized from water soluble calcium salt [24]. Chemical transformation may also contribute to these changes. In order to better understand the thermal effect on the properties of the solids, SEM observation, particle size distribution, and TMA were performed.

SEM, particle size distribution, and TMA

Figure 6 presents SEM images of SYN-K solids dried or calcined at 105–600 °C. The solid dried at 105 °C showed a large range of particle sizes (100 µm scale). At higher magnification (5 µm scale), the porous structure of the particles was clearly observed, which could provide an explanation for the high S_{BET} of this solid. Some slight changes could be observed on the surface of the particles after the calcination at 400 °C. The surface of particles seemed to be more compact and less porous. At 600 °C, the appearance of particles considerably changed. They became much more rounded in comparison with the particles of the solid dried at 105 °C. The surface of particles completely changed too, which was probably due to the chemical trans-

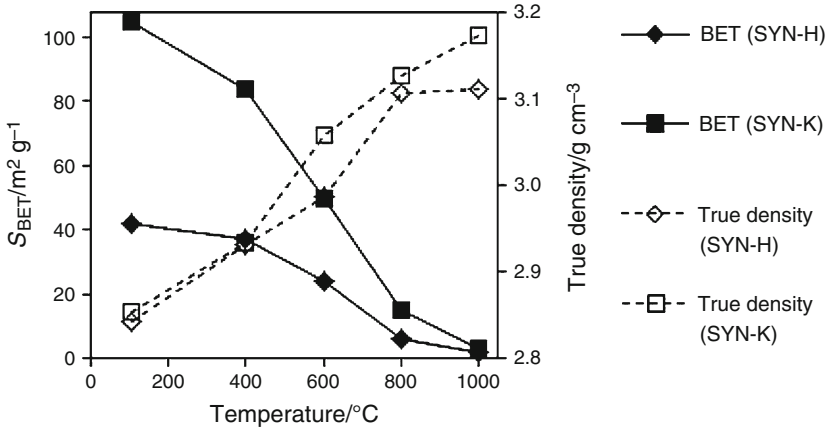

Fig. 5 Influence of the calcination temperature on the specific surface area and true density

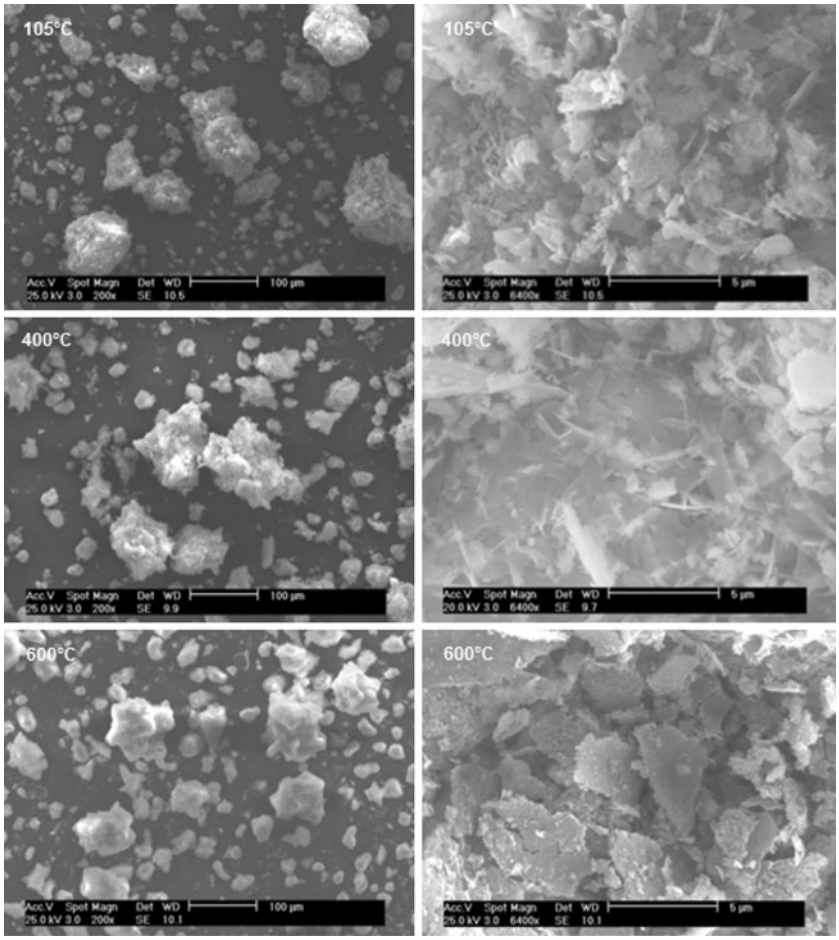

Fig. 6 SEM *images* of SYN-K solids treated at 105–600 °C

formations in the mass of the solid, such as the decomposition of calcite.

In Fig. 7, the surface of SYN-H solid dried at 105 °C seems to be compact, with a high occurrence of particles of sheet-like structure. The latter could be due to the higher content of DCPD and DCPA present in this solid, as found in TG analysis [25–27]. At 400 °C, particles of sheet-like structure remained because DCPA decomposed at a higher temperature (about 430 °C) [28, 29]. At 600 °C, a transformation on the surface of particles was also observed, which was related to the chemical reactions, with the disappearance of DCPD, DCPA, and calcite, and the formation of calcium pyrophosphate and calcium oxide as new intermediates (Fig. 2).

Figure 8 presents SEM images of the solids from both SYN-H and SYN-K syntheses, which were calcined at 800 and 1,000 °C. The sintering phenomenon was clearly observed, where growing necks merged. At these temperatures, particles became more rounded and their surface was smoother in comparison with the particles of the solids treated at lower temperatures. The sintering seemed to be more important with SYN-H solid than with SYN-K solid. This result was probably related to the thermal decomposition of $CaCO_3$ where released carbon dioxide could form a layer of gas in the porous structure or in the interparticle pores of the solids, resulting in a decrease in the sintering rate. In addition to the effect of released CO_2 gas, the formation of CaO as solid product of this decarbonation might also slow down the sintering rate, as previously observed for the sintering of silicon carbide [30]. Accordingly, the dried SYN-H solid, with lower content of residual calcium carbonate (Table 2), sintered more than the dried SYN-K.

For both solids, an increase in particle size was observed when the calcination temperature changed from 800 to 1,000 °C. Static laser light scattering was then carried out to better understand the change of the particle size under thermal effect (Fig. 9).

The initial calcium carbonate used in this study had the median diameter (d_{50}) of 13.2 and 23.3 μm for particle number and volume size distributions, respectively. For the volume distributions of the SYN-H solids, a wide particle-size distribution was observed in the range of 0.3–500 μm. For the solids treated at 105–800 °C, three populations of

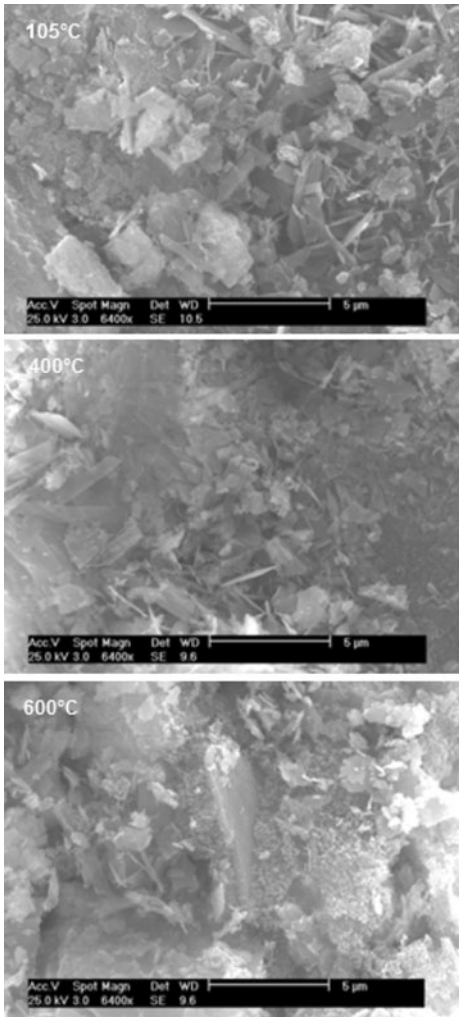

Fig. 7 SEM *images* of the solid issue from SYN-H treated at 105–600 °C

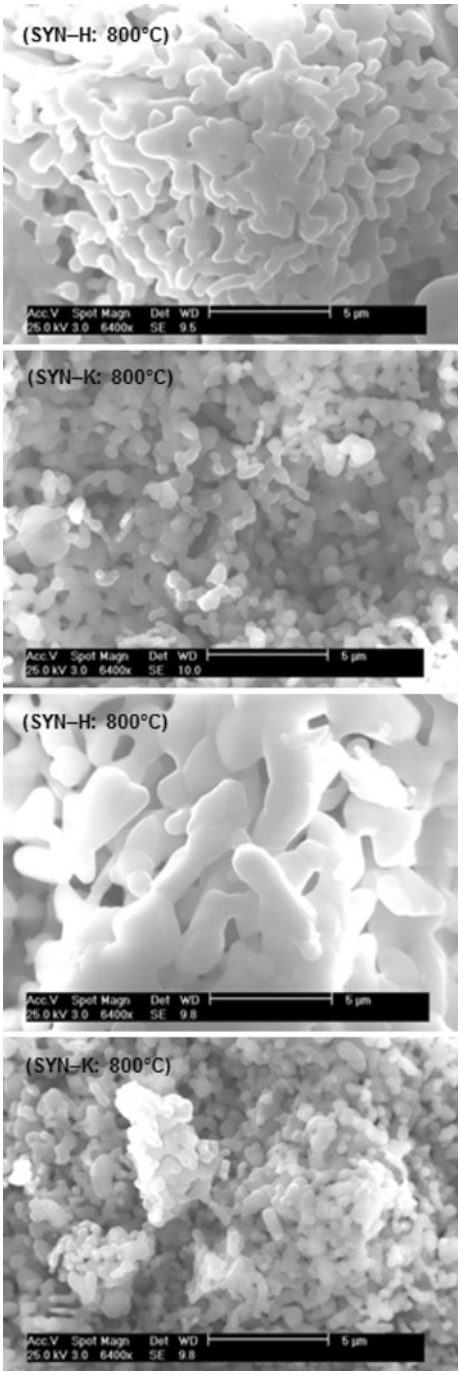

Fig. 8 SEM *images* of both solids SYN-H and SYN-K calcined at 800–1,000 °C

sizes (trimodal peaks) could be clearly observed, which were of approximately 0.3–1, 1–30, and 30–500 μm. The calcination at 1,000 °C mostly eliminated particles smaller than 2.5 μm and a monomodal-like peak appeared in the range of 2.5–300 μm.

Similar results were obtained for the volume distribution of the SYN-K solids. However, the particle-size distribution was found in a narrower range of 0.3–300 μm, which was in accord with SEM results. Three populations of sizes of approximately 0.3–1, 1–6, and 6–300 μm were observed. The calcination at 1,000 °C also led to the elimination of particles smaller than 1.8 μm and a bimodal peak appeared. In all cases, the highest volume fractions were found for the populations of the largest particles (30–500 μm for SYN-H and 6–300 μm for SYN-K solids).

In contrast with the volume distributions, the number distributions changed completely. At 105–800 °C, monomodal peaks appeared and more than 95 % of particles were found in the population of sizes from 0.3 to 1 μm. The number of particles larger than 3 μm was practically negligible. At 1,000 °C, the effect of thermal treatment was distinct with the displacement of the monomodal peaks to the ranges of 2–30 μm for SYN-H solid and 1.6–30 μm for SYN-K solid.

The analysis of particle size distribution also showed that, despite a great number of fine particles, their volumes

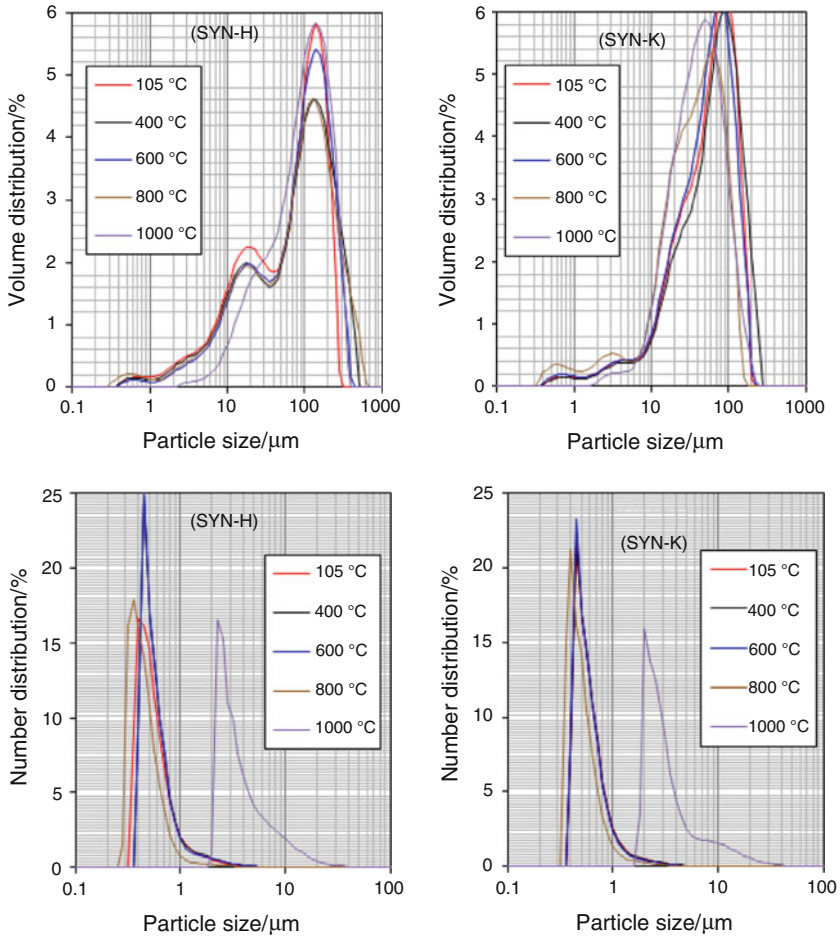

Fig. 9 Influence of the calcination temperatures on the particle-size distributions; *x* axis value is in logarithm to base 10 scale

were modest. Table 4 shows the number and volume accumulations of the solids calcined at 1,000 °C. There were less than 8 % of particles of sizes larger than 10 μm but their volume was higher than 88 %.

In order to quantify the shrinkage/dilatation of the solids under thermal treatment, TMA of both dried SYN-H and SYN-K solids was carried out.

Thermal shrinkage is defined as $(L - L_o)/L_o$ or $\Delta L/L_o$, where L_o is the initial length of sample, and L is the length of sample measured at temperature T or time t. Figure 10a1, a2 show the non-isothermal TMA curves in the temperature range of 30–1,000 °C, where the solids were heated at the rate of 10 °C min^{-1}. For the dried SYN-H solid, some small deformations were observed at the temperatures lower than 800 °C. Then, a strong shrinkage started at about 800 °C which must be due to the sintering of the solid, and was in coherence with SEM observation (Fig. 8). A shrinkage level of −4.2 % took place from 800 to 1,000 °C. In the similar heating conditions, the dried SYN-K solid started to sinter at lower temperature, which was about 640 °C, and a much higher shrinkage level of −30.2 % was observed in the temperature range of 640–1,000 °C.

Heating of a loose mass generally leads to consolidation or sintering to a denser mass when the temperature reaches a limit. Bailliez and Nzihou [24] graphically illustrated three steps of the sintering process, including the formation and growth of contact areas between adjacent particles; the merging of growing necks and the densification of the solid by destruction of interparticle porosity formed during the second step. In this study, the dried SYN-H solid had the specific surface area (S_{BET}) and the porous volume (V_p), obtained from adsorption–desorption isotherms, of 42 m^2

Table 4 Comparison of number and volume accumulation of particles for solids calcined at 1,000 °C

Solid	SYN-H		SYN-K	
	≤10 μm	>10 μm	≤10 μm	>10 μm
Number accumulation/%	92.0	8.0	92.8	7.2
Volume accumulation/%	5.3	94.7	11.1	88.9

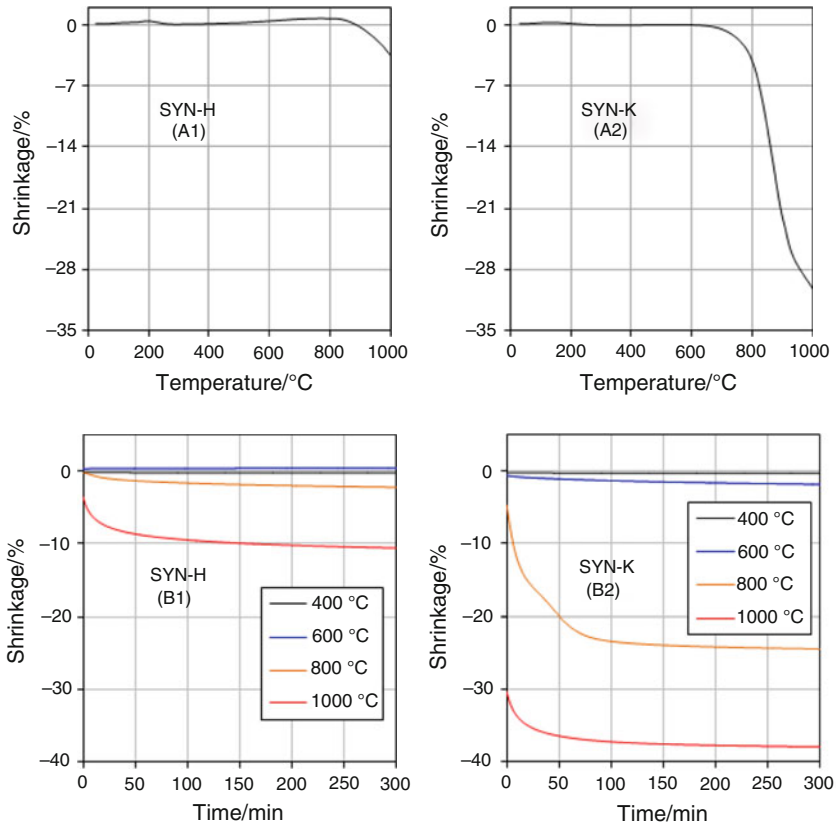

Fig. 10 TMA of the solid products; **a1** and **a2**: non-isothermal shrinkage (heating rate: 10 °C min^{-1}) of the solids dried at 105 °C; **b1** and **b2**: isothermal shrinkage (300 min) of the solids dried at 105 °C

g^{-1} and 0.24 cm^3 g^{-1}, respectively. Those of the dried SYN-K solid were of 103 m^2 g^{-1} and 0.68 cm^3 g^{-1}, respectively. As a function of the calcination temperature, S_{BET} of both solids decreased. After the treatment at 1,000 °C, their S_{BET} were deeply reduced to 2–3 m^2 g^{-1}, which are values characteristic for non-porous solid powders. Thus, it can be assumed that the dried SYN-K solid, with higher porosity, had a more important shrinkage under thermal effect, than the dried SYN-H solid. The higher mass loss by decarbonation of residual calcium carbonate present in the dried SYN-K solid also explained its higher shrinkage (Fig. 1).

Figure 10b1, b2 present the isothermal TMA curves of SYN-H and SYN-K solids at different temperatures. The initial value at time zero of each curve corresponded to the shrinkage of the sample during the heating step to the desired temperature. The isothermal shrinkage was negligible at 400 and 600 °C and was much higher at 800 and 1,000 °C. After a long isothermal time of 300 min, the shrinkage slightly continued even at 1,000 °C. In fact, as observed in Fig. 8, both solids were still at the stage of necks merging, meaning that the sintering had not reach the densification step yet.

Conclusions

Calcium carbonate could directly be used as an unconventional source of calcium for the synthesis of apatitic calcium phosphates. Under ambient conditions, the use of orthophosphoric acid showed more advantages than potassium dihydrogen orthophosphate, thanks to a higher dissolution of calcium carbonate and a better precipitation of orthophosphate species. The use of orthophosphoric acid further prevented formation of waste by-products in the final suspension of the synthesis.

For the first time, the thermal behavior of apatitic calcium phosphates starting from calcium carbonate was investigated. Thermal treatment strongly influenced the physico-chemical properties of the solids including the reduction of specific surface area and the increase of true density and particle size. This was related to the sintering phenomenon of particles and the chemical transformations in the mass of the solids. At 800–1,000 °C, mixtures of well-crystallized Ca-HA and a small amount of TCP (from SYN-H, using orthophosphoric acid) or well-crystallized Ca-HA, CaO, and TCP (from SYN-K, using potassium dihydrogen orthophosphate) were formed.

These results will be considered for our future works on the use of the obtained solid products in high temperature processes including heterogeneous catalysis and treatment of polluted gas.

Acknowledgements The authors gratefully acknowledge the support from Dr. Nathalie Lyczko, Mr. Philippe Accart, Mr. Denis Marty, and Ms. Christine Rolland at the centre RAPSODEE for different measurements.

References

1. Habraken WJEM, Wolke JGC, Jansen JA. Ceramic composites as matrices and scaffolds for drug delivery in tissue engineering. Adv Drug Deliv Rev. 2007;59:234–48.
2. Saha SK, Banerjee A, Banerjee S, Bose S. Synthesis of nanocrystalline hydroxyapatite using surfactant template systems: role of templates in controlling morphology. Mater Sci Eng C. 2009;29:2294–301.
3. Baillez S, Nzihou A, Bernache-Assolant D, Champion E, Sharrock P. Removal of aqueous lead ions by hydroxyapatites: equilibria and kinetic processes. J Hazard Mater. 2007;A139: 443–6.
4. Bianco A, Cacciotti I, Lombardi M, Montanaro L, Gusmano G. Thermal stability and sintering behaviour of hydroxyapatite nanopowders. J Therm Anal Calorim. 2007;88:237–43.
5. De Campos M, Muller FA, Bressiani AHA, Bressiani JC, Greil P. Sonochemical synthesis of calcium phosphate powders. J Mater Sci Mater Med. 2007;18:669–75.
6. Zyman ZZ, Tkachenko MV, Polevodin DV. Preparation and characterization of biphasic calcium phosphate ceramics of desired composition. J Mater Sci Mater Med. 2008;19:2819–25.
7. Saeki T. A new type of CO_2 gas sensor comprising porous hydroxyapatite ceramics. Sens Actuators. 1998;15:145–51.
8. Boukha Z, Kacimi M, Pereira MFR, Faria JL, Figueiredo JL, Ziyad M. Methane dry reforming on Ni loaded hydroxyapatite and fluoroapatite. Appl Catal A. 2007;317:299–309.
9. Khachani M, Kacimi M, Ensuque A, Piquemal JY, Connan C, Bozon-Verduraz F, Ziyad M. Iron–calcium–hydroxyapatite catalysts: iron speciation and comparative performances in butan-2-ol conversion and propane oxidative dehydrogenation. Appl Catal A. 2010;388:113–23.
10. Pham Minh D, Sebei H, Nzihou A, Sharrock P. Apatitic calcium phosphates: synthesis, characterization and reactivity in the removal of lead(II) from aqueous solution. Chem Eng J. 2012;198–199:180–90.
11. Kim DW, Cho IS, Kim JY, Jang HL, Han GS, Ryu HS, Shin H, Jung HS, Kim H, Hong KS. Simple large-scale synthesis of hydroxyapatite nanoparticles: in situ observation of crystallization process. Langmuir. 2010;26:384–8.
12. Elliott JC. Structure and chemistry of the apatites and other calcium orthophosphates. In: Studies in inorganic chemistry, vol 18. Amsterdam: Elsevier; 1994.
13. El Feki H, Khattech I, Jemal M, Rey C. Décomposition thermique d'hydroxyapatites carbonatées sodées. Thermochim Acta. 1994;237:99–110.
14. Tônsuaadu K, Peld M, Leskela T, Mannonen R, Niinisto L, Veiderma M. A thermoanalytical study of synthetic carbonate-containing apatites. Thermochim Acta. 1995;256:55–65.
15. Wilson RM, Elliott JC, Dowker SEP, Smith RI. Rietveld structure refinement of precipitated carbonate apatite using neutron diffraction data. Biomaterials. 2004;25:2205–13.
16. Yao F, LeGeros JP, LeGeros RZ. Simultaneous incorporation of carbonate and fluoride in synthetic apatites: effect on crystallographic and physico-chemical properties. Acta Biomater. 2009;5: 2169–77.
17. Landin M, Rowe RC, York P. Particle size effects on the dehydration of dicalcium phosphate dihydrate powders. Int J Pharm. 1994;104:271–5.
18. Yoğurtcuoğlu E, Uçurum M. Surface modification of calcite by wet-stirred ball milling and its properties. Powder Technol. 2011;214:47–53.
19. Vagenas NV, Gatsouli A, Kontoyannis CG. Quantitative analysis of synthetic calcium carbonate polymorphs using FT-IR spectroscopy. Talanta. 2003;59:831–6.
20. Gunasekaran S, Anbalagan G. Spectroscopic study of phase transitions in natural calcite mineral. Spectrochim Acta. 2008; A69:1246–51.
21. Karlinsey RL, Mackey AC, Walker ER, Frederick KE. Preparation, characterization and in vitro efficacy of an acid-modified β-TCP material for dental hard-tissue remineralization. Acta Biomater. 2010;6:969–78.
22. Coelho PG, Coimbra ME, Ribeiro C, Fancio E, Higa O, Suzuki M, Marincola M. Physico/chemical characterization and preliminary human histology assessment of a β-TCP particulate material for bone augmentation. Mater Sci Eng C. 2009;29:2085–91.
23. Koumoulidis GC, Trapalis CC, Vaimakis TC. Sintering of hydroxyapatite lath-like powders. J Therm Anal Calorim. 2006; 84:165–74.
24. Bailliez S, Nzihou A. The kinetics of surface area reduction during isothermal sintering of hydroxyapatite adsorbent. Chem Eng J. 2004;98:141–52.
25. Arifuzzaman SM, Rohani S. Experimental study of brushite precipitation. J Cryst Growth. 2004;267:624–34.
26. Stulajterova R, Medvecky L. Effect of calcium ions on transformation brushite to hydroxyapatite in aqueous solutions. Colloids Surf A. 2008;316:104–9.
27. Jinawath S, Sujaridworakun P. Fabrication of porous calcium phosphates. Mater Sci Eng C. 2002;22:41–6.
28. Frost RL, Palmer SJ. Thermal stability of the 'cave' mineral brushite $CaHPO_4{\cdot}2H_2O$—mechanism of formation and decomposition. Thermochim Acta. 2011;521:14–7.
29. Mitsionis AI, Vaimakis TC. A calorimetric study of the temperature effect on calcium phosphate precipitation. J Therm Anal Calorim. 2010;99:785–9.
30. Zawrah MF, Shaw L. Liquid-phase sintering of SiC in presence of CaO. Ceram Int. 2004;30:721–5.